Supporting Information for

Hierarchical 2D-1D Micelles Self-Assembled from Heterogeneous Seeded-Growth of Rod-Coil Block Copolymers

Chengyan Zhang, Liang Gao, Jiaping Lin*, and Liquan Wang*

Shanghai Key Laboratory of Advanced Polymeric Materials, Key Laboratory for Ultrafine Materials of Ministry of Education, Frontiers Science Center for Materiobiology and Dynamic Chemistry, School of Materials Science and Engineering, East China University of Science and Technology, Shanghai 200237, China

* Corresponding Authors. E-mail: lianggao@ecust.edu.cn (L.G.); jlin@ecust.edu.cn (J.L.)

Contents

1. Theoretical Simulations ..... SI 3

1.1 Brownian dynamics simulation method..... SI 3

1.2 Parameters settings..... SI 5

1.3 Calculation of the number of cylindrical arms and active areas. ..... SI 6

1.4 Calculation of the diffusion coefficients ..... SI 7

2. Seed formation from self-assembly of rod-coil block copolymers..... SI 8

3. Three kinds of growth manners of disklike micelles ..... SI 11

4. Effect of added unimer concentration on the growth of hybrid micelles..... SI 13

5. Effect of the disk seed size on the arm number ..... SI 14

References..... SI 16

1. Theoretical Simulations

1.1 Brownian dynamics simulation method

The Brownian dynamics (BD) simulation was developed by Grest and Kremer,[S1, S2] which is an efficient method for simulating polymer self-assembly. The BD simulation can well realize the implicit description of the continuum solvent and the simplification of internal motions. The temporal evolution of the beads obeys the Langevin equation, including all the potentials, the friction term, and the noise term. The beads are coupled to a heat bath, and the equation of motion is written as

$$m_i \frac{d^2\mathbf{r}_i}{dt^2} = \mathbf{F}_i - \Gamma_0 \frac{d\mathbf{r}_i}{dt} + \mathbf{W}_i(t) \tag{S-1}$$

where m_i is the mass of the i-th bead, Γ_0 is the friction constant, and $\mathbf{F}_i$ is the force acting on the i-th bead, which can be obtained by the derivatives of U_{mol} and U_{ij}. $\mathbf{W}_i(t)$ can be calculated through the fluctuation-dissipation relation

$$\left\langle \mathbf{W}_i(t) \cdot \mathbf{W}_j(t') \right\rangle = 6k_{\mathrm{B}}T\Gamma_0\delta_{ij}\delta(t-t') \tag{S-2}$$

In the simulation, the periodic boundary conditions are imposed. The integration time step $\Delta t = 0.005\,\tau$, and the simulation temperature $k_{\mathrm{B}}T = 3.0\varepsilon$ was selected.[S3-S5] Here, $\tau = (m\sigma^2/\varepsilon)^{1/2}$ is the time unit, m is the unit of mass, σ is the unit of length, and ε is the unit of energy.

We consider a simulation system consisting of rod-coil block copolymers in implicit solvents. The copolymers are modeled as linear chains with **R** beads of rod block and **C** beads of coil block, denoted by $\mathbf{R_mC_n}$ (the subscripts m and n denote the bead number of each block), as shown in Figure S1A. In the coarse-grained copolymer model, one bead represents a cluster of atoms or repeat units. The coarse-grained model is parameterized based on experiments. By mapping multiple real atoms into an interaction site, the model can correspond to a block copolymer chain.[S6]

The bead-bead interactions are given by the bonding potential U_{mol} and the nonbonding potential U_{ij}. The U_{mol} can maintain a desired molecular chain structure, while the U_{ij} describes the nonbonding interactions. For the rod blocks, the U_{mol} can be divided into two parts, that is, the bond stretching potential U_{bond} and the angle bending potential U_{angle}. All the neighboring beads are connected by a bond model with a harmonic spring potential, given by

$$U_{bond}(r) = \frac{1}{2} k_b (r - r_0)^2 \tag{S-3}$$

where k_b is the bond spring constant, r is the distance between the chemically bonded beads, and r_0 is the equilibrium bond length. To realize the rigidity of the rod blocks, the angle bending potential is introduced

$$U_{angle}(\theta) = \frac{1}{2} k_a (\theta - \theta_0)^2 \tag{S-4}$$

where k_a is the angle spring constant, θ is the angle between two neighboring bonds, and θ_0 is the equilibrium angle.

The nonbonding potential U_{ij} between any pair of i-th and j-th beads is given by the standard Lennard-Jones (LJ) potential

$$U_{ij} = \begin{cases} 4\varepsilon_{ij}\left[\left(\frac{\sigma}{r_{ij}}\right)^{12} - \left(\frac{\sigma}{r_{ij}}\right)^{6} - \left(\frac{\sigma}{r_{ij}^c}\right)^{12} + \left(\frac{\sigma}{r_{ij}^c}\right)^{6}\right], & r \le r_{ij}^c \\ 0, & r > r_{ij}^c \end{cases} \tag{S-5}$$

where $r_{ij} = \left|\mathbf{r}_i - \mathbf{r}_j\right|$ with $\mathbf{r}_i$ and $\mathbf{r}_j$ being the positions of the i-th and j-th beads, respectively. r_{ij}^c is the cutoff distance, and ε_{ij} is the interaction parameter between the i-th and j-th beads.

The simulations are performed by applying the simulator, coarse-grained molecular dynamics program based on LAMMPS.[S7]

1.2 Parameters settings

Bond and angle. All the neighboring beads are connected by a bond model with a harmonic spring potential, which is given by Eqn.(S-3). The equilibrium bond length r_0 is 1.0σ for the rod and coil blocks. The value of k_b is set as 100 ε/σ^2 to avoid the over-stretching of bonds. To model the rigidity of rod blocks, the angle bending potential is introduced by Eqn.(S-4). In the simulations, the angle bending potential is employed by setting the angle spring constant $k_a = 100\varepsilon$ and $\theta_0 = 180°$ for the rod block, while for the coil block, $k_a = 0$.

Cutoff radius. To take account of the solvent selectivity, the cutoff distance rules of the LJ potential Eqn.(S-5) are defined as follows. For the hydrophilic coil blocks, the **C-C** interactions are effectively repelled from each other by setting r_{CC}^c as $2^{1/6}\sigma$. While the **R-R** interactions are effectively attracted to each other by setting r_{RR}^c as 2.5σ. To simulate the immiscibility between the rod and coil blocks, r_{RC}^c is set as $2^{1/6}\sigma$. [S8]

Interaction parameters and simulation time. To simulate **R-C** and **C-C** interactions, the pairwise interaction parameters are set as follows, $\varepsilon_{RC} = \varepsilon_{CC} = 1.0\varepsilon$. The higher hydrophobicity is simulated by the stronger interaction strength ε_{RR} between the **R** and **R** beads. For the construction of disk seeds, the aggregates are self-assembled from the $\mathbf{R_mC_n}$ copolymers at the interaction parameters ε_{RR} of 3.0ε. BD simulations with 1.0×10^8 steps ($5.0\times10^5\,\tau$) are carried out so that the simulation time is long enough for the system to achieve an equilibrium state. In the seeded-growth process, the copolymer chains are put into a simulation box containing the disklike seeds obtained in the first step ($C_0 = 1.0\times10^{-3}\sigma^{-3}$ and $\varepsilon_{RR} = 3.0\varepsilon$). The unimers (for example, $C_0^{2nd} = 1.0\times10^{-4}\,\sigma^{-3}$, *i.e.*, 338 unimers in the simulation box) are added into the seed solution, and the contour area of the initial disk seeds is fixed at $240\sigma^2$, and the

interaction parameter ε_{RR} is varied from 2.2ε to 2.8ε. BD simulations with 2.0×10^7 steps ($1.0\times10^5\tau$) are chosen to observe the growth process, which is long enough for the system to get equilibrium.

Simulation box. All the simulations are performed in a cubic cell using a dynamic algorithm with the temperature controlling method (NVT ensemble). For the construction of disk seeds, the box size is set as $60\times60\times60\ \sigma^3$. In the seeded-growth stage, the simulation box is set as $150\times150\times150\ \sigma^3$.

1.3 Calculation of the number of cylindrical arms and active areas.

The hybrid disk-cylinder micelles, with a disk region and cylindrical arms, are assembled *via* a seeded-growth manner. The rod blocks form the core of hybrid disk-cylinder micelles, while the coil blocks in the corona stabilize the micelle structures. The diameter D of the arms is determined by the rod block length according to the cholesteric-like LC structure core in the arms. For the $\mathbf{R_6C_3}$ copolymers, D is about 5.0σ. The length of cylindrical arms L in the hybrid micelles is defined by the distance from the disk region edges to the cylindrical arm ends (see Scheme S1A).

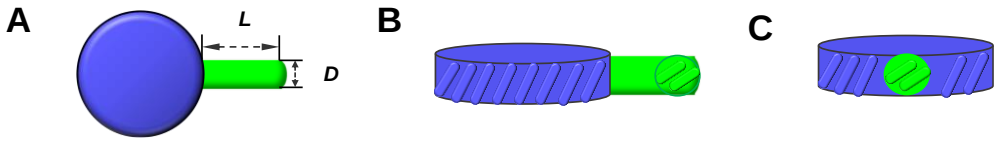

Scheme S1. Sketch of the hybrid disk-cylinder micelle, (A) top view, (B) side view, (C) front view.

The chain packing of copolymers is inclined in the disk seed edges, and the exposed rod blocks are regarded as the active sites (see Scheme S1B, C). In the initial growth stage, the growth occurs at the disk seed edges. The rod blocks at disk seed edges serve as the active sites. As the growth progresses, the active sites transform from the disk seed edges to the cylindrical arm ends (Figure 2). We defined the ratio of the number of exposed rod blocks at the disk seed edges or the arm ends to the system volume as the concentration C_{active}.

1.4 Calculation of the diffusion coefficients

The diffusion behavior of the hybrid disk-cylinder micelles is evaluated by calculating the diffusion coefficients of the center-of-mass (D_{cm}) and the arm ends (D_{end}). The motions of chain beads in the center or the edge regions are traced to evaluate their displacements. The mean square displacements (MSDs) of arm ends are defined as the MSDs of all the copolymer beads within 1σ from the arm end. The average value of the MSDs of these beads is calculated to describe the motion of arm ends. The diffusion coefficients of the center-of-mass of the disklike micelle are calculated as well. The diffusion coefficients are related to the MSDs of corresponding motion units, which can be calculated by the Einstein relation[S9]

$$D = \lim_{t\to\infty} \frac{dMSD(t)}{6dt} \tag{S-6}$$

$$MSD(t) = \left\langle [\mathbf{r}(t_0 + t) - \mathbf{r}(t_0)]^2 \right\rangle \tag{S-7}$$

where $\mathbf{r}(t_0 + t)$ and $\mathbf{r}(t_0)$ are the positions of the particles at t+t_0 and t_0, respectively.

For the comparison of diffusion behavior of the hybrid micelle and disklike micelle, the chain number of $\mathbf{R_6C_3}$ copolymers in the micelles is kept the same (*appr.* 560 copolymer chains). For the calculation of diffusion behavior of various hybrid micelles, the area of the disk region and the total length of the cylindrical arms are constant, all the hybrid micelles contain 550~600 copolymer chains, and the number of the cylindrical arms is regulated.

2. Seed formation from self-assembly of rod-coil block copolymers

Block copolymers with hydrophobic rod block and hydrophilic coil block are constructed. The copolymers are modeled as linear chains with **R** beads of the rod block and **C** beads of the coil block, denoted as $\mathbf{R_mC_n}$ (the subscripts *m* and *n* denote the bead number of each block). As shown in Figure S1A, the **R** and **C** beads are denoted with blue and red colors, respectively. To choose the suitable coarse-grained copolymer model for the formation of 2D seeds and the subsequent 1D growth, we examined the self-assembly behaviors of the $\mathbf{R_mC_n}$ block copolymer with various block ratios. The copolymer concentration C_0 and interaction strength ε_{RR} are fixed at $1.0\times10^{-3}\,\sigma^{-3}$ and 2.5ε, respectively.

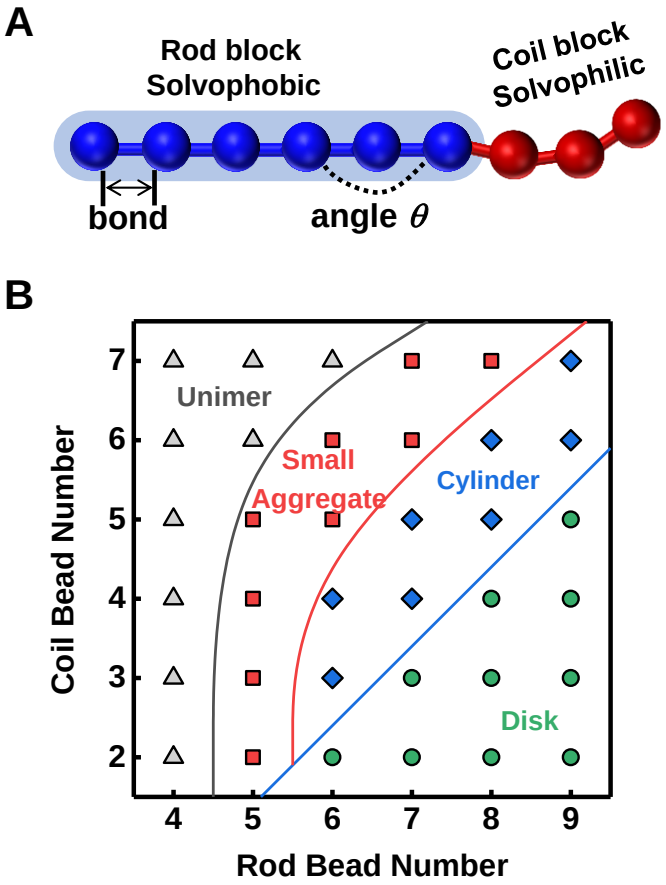

Figure S1. (A) BD model of a rod-coil block copolymer, which is denoted as $\mathbf{R_6C_3}$. (B) Morphological diagram of the aggregates formed by $\mathbf{R_mC_n}$ copolymers. All the stable self-assembled structures are obtained at the simulation time of $5.0\times10^5\ \tau$.

The simulation results obtained at various bead numbers m and n are summarized into a morphological diagram shown in Figure S1B. It was found that the $\mathbf{R_mC_n}$ copolymers can self-assemble into small aggregates, cylindrical micelles, and disklike micelles. As the bead number m is small (*i.e.,* short rod block), the copolymers exist as unimers. When varying the rod-to-coil block ratio by increasing the length of rod blocks, small aggregates and disklike micelles are assembled from the copolymers with longer coil blocks and shorter coil blocks, respectively. The $\mathbf{R_6C_3}$ copolymers have medium lengths of rod and coil blocks, and they can assemble into either cylindrical micelles or disklike micelles. Therefore, the $\mathbf{R_6C_3}$ copolymers are chosen to construct the disk seed and investigate the growth of hybrid disk-cylinder micelles in this work.

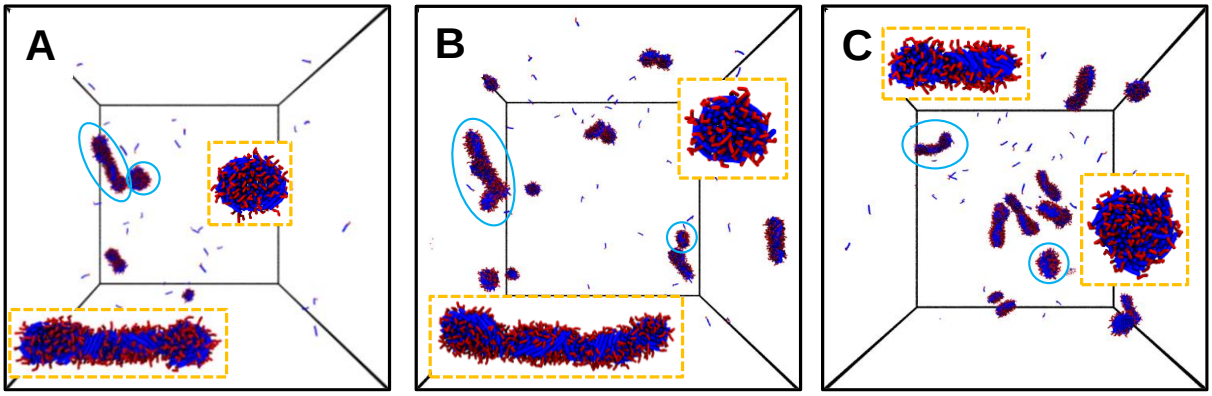

Figure S2. Typical simulation snapshots are obtained from the transition region (pink region) in Figure 1B in the main text, where the interaction strength ε_{RR} is fixed at 3.1ε and the simulation time is $5.0\times10^5\tau$. The concentration of initial copolymers C_0 is (A) $1.0\times10^{-4}\sigma^{-3}$, (B) $2.0\times10^{-4}\sigma^{-3}$, (C) $3.0\times10^{-4}\sigma^{-3}$, respectively. The dashed box is an enlarged view of the circled micelle structures.

The morphologies of the $\mathbf{R_6C_3}$ block copolymers are also determined by the interaction strength ε_{RR} between the rod blocks and the initial concentration C_0 of the copolymers. With increasing the interaction ε_{RR}, cylindrical micelles and disklike micelles are obtained. Note that the transformation process from the cylindrical micelles to the disklike micelles is not a first-order phase transition. Thus, there is a transition region between the cylindrical morphological phase and the disklike morphological

phase. Typical simulation snapshots for various C_0 at the given ε_{RR} in the transition phase region are illustrated in Figure S2. Almost all unimers assemble into the aggregates. The cylindrical micelles and the disklike micelles simultaneously exist in the phase transition region (dashed box in Figure S2). As the C_0 increases, the concentration of the cylindrical and the disklike micelles gradually increases. The phase transition region provides a possibility for constructing hybrid disk-cylinder micelles *via* a seeded-growth manner.

3. Three kinds of growth manners of disklike micelles

Living growth of disklike micelles. The unimers are added to the disk seed solution (disk seed form at $C_0 = 1.0\times10^{-3}\ \sigma^{-3}$ and $\varepsilon_{RR} = 3.0\varepsilon$). The rod blocks in the disk seed and the newly added unimers are blue and green, respectively (Figure S3A). When the C_0^{2nd} and the interaction strength ε_{RR} are relatively low (*e.g.*, C_0^{2nd} and ε_{RR} are fixed at $1.0\times10^{-4}\sigma^{-3}$ and 2.5ε, respectively), the disklike micelles are obtained. As shown in Figure S3B-D, no new aggregates are formed in the system, and the unimers incorporate onto the disk edges one by one. With increasing the simulation time, almost all unimers grow on the seed, and the larger concentric disklike micelle can be constructed. This growth process exhibits characteristics of living growth.[S10]

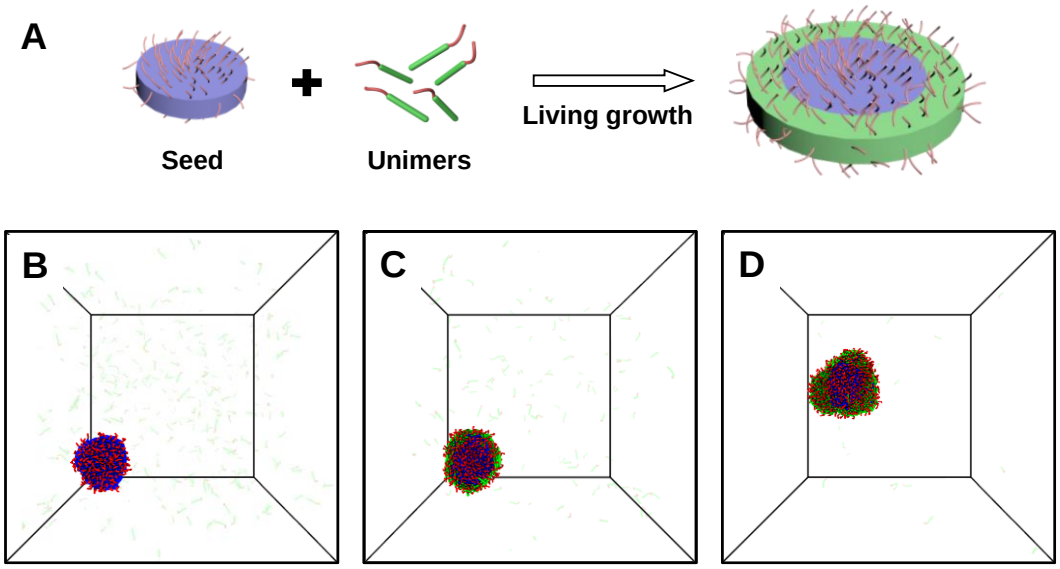

Figure S3. (A) The disklike micelles are formed by the **R_6C_3** copolymers in a seeded-growth manner *via* the living growth process. The simulation time is (B) 0 τ, (C) $2.5\times10^4\tau$, (D) $1.0\times10^5\tau$, respectively.

Fusion growth of disklike micelles. The disklike micelles can also be constructed at the higher C_0^{2nd} and the interaction strength ε_{RR}. For example, the C_0^{2nd} and ε_{RR} are fixed at $5.0\times10^{-4}\sigma^{-3}$ and 3.0ε, respectively. This growth process is illustrated in Figure S4A. Most of the added unimers tend to form

primary small aggregates at first (Figure S4C). The newly formed aggregates have a certain exposed area that can contact the edge of the disk seeds and fuse with the seed. As the simulation time increases, more aggregates grow onto the disk seed. Meanwhile, the rod blocks in the aggregate adjust themselves to match the chain arrangement of the seed micelle, and the larger disklike micelle can be obtained *via* the fusion growth process. (Figure S4B-D).[S11]

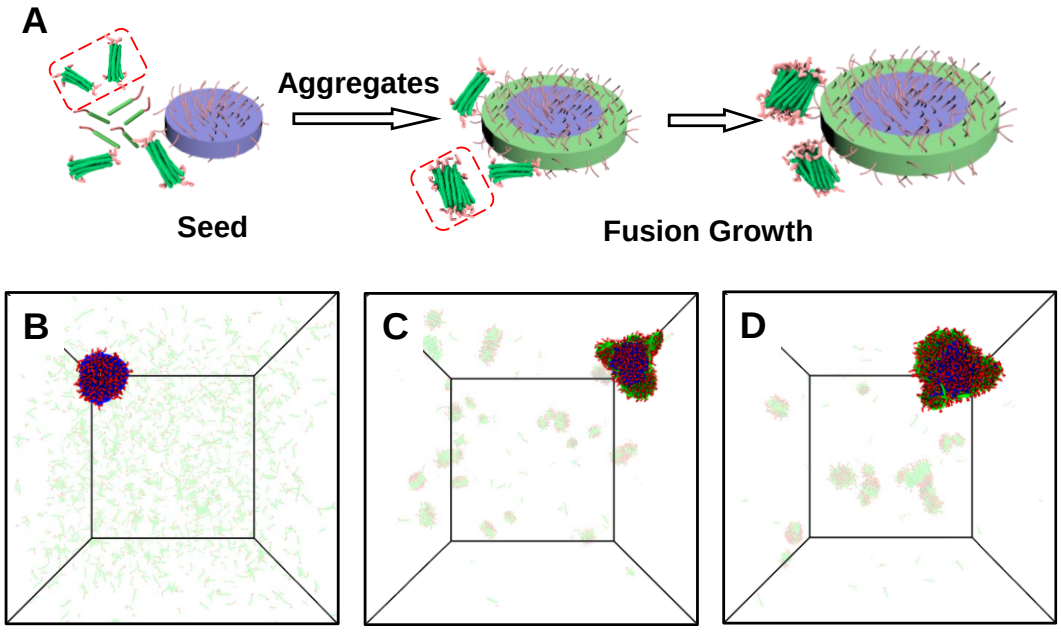

Figure S4. (A) The disklike micelles are formed by the **R_6C_3** copolymers in a seeded-growth manner *via* a fusion growth process. The simulation time is (B) 0 τ, (C) 2.5×10^4 τ, (D) 1.0×10^5 τ, respectively.

Hybrid growth of disklike micelles. Under the conditions of moderate ε_{RR}, the added unimers are attached to the disk seed edges, but they cannot adjust themselves to well match the LC-like structures in the seeds. With simulation time increasing, the attached unimers assemble into 1D cylindrical structures (*i.e.*, the arms of seeds), and then the hybrid disk-cylinder (2D-1D) structures are formed (see Figure 2A-D in the main text). Unlike the 2D living growth and the 2D fusion growth manners, we termed such a growth behavior as a 2D-1D hybrid growth manner.

4. Effect of added unimer concentration on the growth of hybrid micelles

The effect of the added unimer concentration C_0^{2nd} on the growth of hybrid disk-cylinder micelles is examined. The ε_{RR} is fixed at 2.5, and the C_0^{2nd} is varied from $2.0\times10^{-4}\sigma^{-3}$ to $6.0\times10^{-4}\sigma^{-3}$. The size of the initial disk seeds is *ca.* $240\sigma^2$, and the simulation time is $1.0\times10^5\tau$ for equilibrium. Figure S5A-E displays the typical simulation snapshots of the hybrid disk-cylinder micelles at various C_0^{2nd}. For the higher C_0^{2nd}, the hybrid disk-cylinder micelles with longer cylindrical arms can be observed. Meanwhile, the arm number on the hybrid disk-cylinder micelles at various C_0^{2nd} is examined. For the fixed C_0^{2nd}, the small error bars indicate the weak fluctuation in the arm number. As the C_0^{2nd} increases, the arm number is basically the same (Figure S5F). These results demonstrate that C_0^{2nd} has less effect on the arm number under the present condition employed.

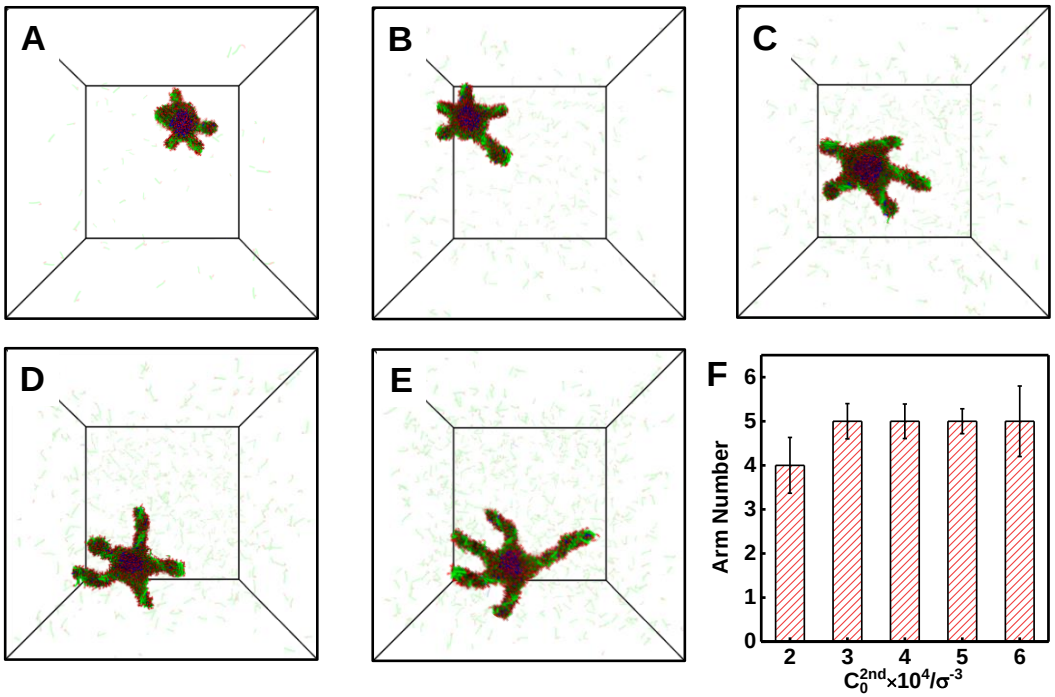

Figure S5. Typical simulation snapshots of the hybrid disk-cylinder micelles, where the interaction strength ε_{RR} is fixed at 2.5ε and the simulation time is $1.0\times10^5\tau$. The concentration of added unimers C_0^{2nd} is (A) $2.0\times10^{-4}\sigma^{-3}$, (B) $3.0\times10^{-4}\sigma^{-3}$, (C) $4.0\times10^{-4}\sigma^{-3}$, (D) $5.0\times10^{-4}\sigma^{-3}$, (E) $6.0\times10^{-4}\sigma^{-3}$, respectively. (F) The arm number on the hybrid disk-cylinder micelles at various C_0^{2nd}.

5. Effect of the disk seed size on the arm number

The effect of the disk seed size on the arm number is examined, where the ε_{RR} and the C_0^{2nd} are fixed at 2.5 and $5.0\times10^{-4}\sigma^{-3}$, respectively. The simulation time is $1.0\times10^{5}\tau$ for equilibrium. Figure S6A shows the morphologies of hybrid disk-cylinder micelles obtained at various disk seed sizes. For the larger disk seed, the more exposed edges are beneficial to the growth of cylindrical arms. As the seed size increases, the arm number increases.

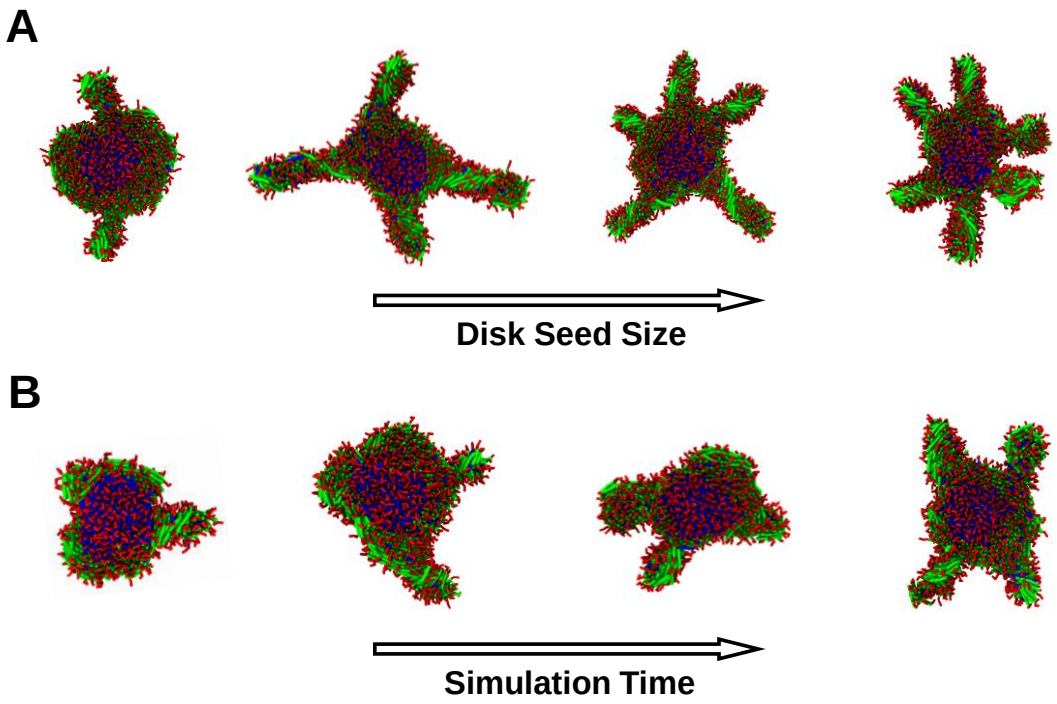

Figure S6. Typical simulation snapshots of the hybrid disk-cylinder micelles with various seed sizes, where the interaction strength ε_{RR} is fixed at 2.5ε and the concentration of added unimers C_0^{2nd} is $5.0\times10^{-4}\sigma^{-3}$, respectively. (A) The area of the disk seed is $120\sigma^2$, $180\sigma^2$, $240\sigma^2$ and $300\sigma^2$, respectively. The simulation time is $1.0\times10^{5}\tau$. (B) The simulation time is $6.0\times10^{3}\tau$, $7.0\times10^{3}\tau$, $8.0\times10^{3}\tau$, and $9.0\times10^{3}\tau$, respectively. The area of the initial disk seed is $240\sigma^2$.

The influence of simulation time on the number and location of cylindrical arms is also examined, where the ε_{RR} and the C_0^{2nd} are fixed at 2.5 and $5.0\times10^{-4}\sigma^{-3}$, respectively. The area of the disk seed is *ca.* $240\sigma^2$. As shown in Figure S6B, in the growth process, the newly grown cylindrical arms tend to

grow in the location that is farthest from the former cylindrical arms due to the steric hindrance effect. For instance, two cylindrical arms grow at the nearly opposite position on the hybrid disk-cylinder micelle when the simulation time is $7.0\times10^3\,\tau$. As the simulation progresses, the cylindrical arms grow on the disk seed edges one by one. For a thermodynamically stable hybrid disk-cylinder micelle, the location of cylindrical arms is uniformly distributed on the disk edges, which is an arrangement that minimizes the energy of the micelles.

References

(S1) Grest, G. S.; Kremer, K., Molecular Dynamics Simulation for Polymers in the Presence of a Heat Bath. *Phys. Rev. A.* **1986,** *33*, 3628-3631.

(S2) Grest, G. S.; Lacasse, M. D.; Kremer, K.; Gupta, A. M., Efficient Continuum Model for Simulating Polymer Blends and Copolymers. *J. Chem. Phys.* **1996,** *105*, 10583-10594.

(S3) Ding, W.; Lin, S.; Lin, J.; Zhang, L., Effect of Chain Conformational Change on Micelle Structures: Experimental Studies and Molecular Dynamics Simulations. *J. Phys. Chem. B* **2008,** *112*, 776-783.

(S4) Horsch, M. A.; Zhang, Z.; Glotzer, S. C., Self-Assembly of Polymer-Tethered Nanorods. *Phys. Rev. Lett.* **2005,** *95*, 056105.

(S5) Lin, S.; Numasawa, N.; Nose, T.; Lin, J., Brownian Molecular Dynamics Simulation on Self-Assembly Behavior of Rod−Coil Diblock Copolymers. *Macromolecules* **2007,** *40*, 1684-1692.

(S6) Srinivas, G.; Shelley, J. C.; Nielsen, S. O.; Discher, D. E.; Klein, M. L., Simulation of Diblock Copolymer Self-Assembly, Using a Coarse-Grain Model. *J. Phys. Chem. B* **2004,** *108*, 8153-8160.

(S7) http://lammps.sandia.gov.

(S8) Zhang, Q.; Lin, J.; Wang, L.; Xu, Z., Theoretical Modeling and Simulations of Self-Assembly of Copolymers in Solution. *Prog. Polym. Sci.* **2017,** *75*, 1-30.

(S9) Einstein, A., Über die von der Molekularkinetischen Theorie der Wärme geforderte Bewegung von in Ruhenden Flüssigkeiten Suspendierten Teilchen. *Ann. Phys.* **1905**, *322*, 549-560.

(S10) Zhang, C.; Lin, J.; Wang, L.; Gao, L., 2D Liquid-Crystallization-Driven Self-Assembly of Rod-Coil Block Copolymers: Living Growth and Self-Similarity. *J. Phys. Chem. Lett.* **2022**, 13, 6215-6222.

(S11) Jin, X.; Zhang, C.; Lin, J.; Cai, C.; Chen, J.; Gao, L., Fusion Growth of Two-Dimensional Disklike Micelles *via* Liquid-Crystallization-Driven Self-Assembly. *Macromolecules* **2022**, 55, 3831-3839.